



# Enhanced room-temperature ammonia vapor-sensing activity of nebulizer spray pyrolysis fabricated SnO<sub>2</sub> thin films: an effect of Er doping

S. Maheswari<sup>1,2</sup>, M. Karunakaran<sup>2,a)</sup>, K. Hariprasad<sup>3</sup>, K. Kasirajan<sup>2</sup>, L. Bruno Chandrasekar<sup>4</sup>, T. Alshahrani<sup>5,a)</sup>, Mohd. Shkir<sup>6,7,a)</sup> , S. AlFaify<sup>7</sup>

<sup>1</sup>Department of Physics, Caussanel College of Arts and Science, Muthupettai, India

<sup>2</sup>PG and Research Department of Physics, Alagappa Govt Arts College, Karaikudi 630003, India

<sup>3</sup>Department of Physics, Institute of Aeronautical Engineering, Dundigal, Hyderabad 500043, India

<sup>4</sup>Department of Physics, Periyar Maniammai Institute of Science & Technology, Vallam, India

<sup>5</sup>Department of Physics, College of Science, Princess Nourah Bint Abdulrahman University, Riyadh 11671, Saudi Arabia

<sup>6</sup>Research Center for Advanced Materials Science (RCAMS), King Khalid University, P.O. Box 9004, Abha 61413, Saudi Arabia

<sup>7</sup>Advanced Functional Materials and Optoelectronic Laboratory (AFMOL), Department of Physics, Faculty of Science, King Khalid University, Abha 61413, Saudi Arabia

<sup>a)</sup>Address all correspondence to these authors. e-mails: shkirphysics@gmail.com; tvdkaruna@gmail.com; thmalshahrani@pnu.edu.sa

Received: 14 August 2020; accepted: 24 November 2020; published online: 4 January 2021

In this work, we have coated 0, 1, 3, and 5 wt% of Erbium (Er)-doped tin oxide (SnO<sub>2</sub>) films on glass using a simple nebulizer spray pyrolysis method to make an ammonia vapor sensor with remarkable sensitivity. X-ray diffraction, Atomic force microscopy, Ultraviolet–visible spectroscopy and photoluminescence methods were employed to inspect the thin-film samples. Room-temperature ammonia vapor sensing was performed by a computer connected to the homemade gas-sensing system. The results obtained show that Er doping in SnO<sub>2</sub> films gradually decreased the crystallite size with an increase of the surface area improving the sensing property of the vapor. A minimum optical band gap (i.e., 3.23 eV) is achieved for 5 wt% Er-doped film. The fabricated Er-doped SnO<sub>2</sub> gas sensor showed response/recovery time highly dependent on dopant concentration. The Er concentration of 5 wt% doped SnO<sub>2</sub> thin film showed maximum sensitivity of 91%, fast response, and recovery time of 29 and 7 s, respectively, due to high surface to volume ratio.

## Introduction

In recent years, air pollution is a major problem due to industrialization and urbanization. All over the world many researchers are focusing their interest in monitoring and preventing air pollution. Most of the researchers used materials like metal oxides, and polymers to solve this major problem. Recently, nanostructured metal oxides are used as a sensor for environmental and biological monitoring due to its excellent properties and also its cost-effectiveness. Shaghayegh Farzi-kahkesh et al. [1], Yanlei Cui et al. [2], and Patil et al. [3] worked on nanostructured metal oxides proved their improved sensing performance toward toxic gases. Ammonia is a natural gas released from agriculture and animal waste, which can affect human, animal, and environmental health. So monitoring and sensing the NH<sub>3</sub> gas is essential

for safety purposes. The metal oxide gas sensors are promising candidates for measuring the parameters regarding air pollution. Some of the metal oxides (MOs) such as ZnO, TiO<sub>2</sub>, WO<sub>3</sub>, and SnO<sub>2</sub> are the materials used for sensing. Among these metal oxides, SnO<sub>2</sub> is an extensively used gas-sensing material. It has n-type with high direct bandgap (~ 3.6 eV), moderate electrical conductivity, low cost, and high-exciton binding energy [4]. Tin oxide crystals show oxygen vacancy and interstitial oxygen atoms that are responsible for the exciting properties of SnO<sub>2</sub> films [5, 6]. It is an utmost striking semiconductor material among the variety of MOs, and has the potential for the detecting the toxic gases [7]. SnO<sub>2</sub>-based gas sensors have been studied for the detection of a variety of gases [8]. Recently Jae-Hun Kim et al. [9] prepared Sb-loaded SnO<sub>2</sub> nanowires which

exhibited better sensing capability due to surface defects. Kelin Hu et al. [10] manufactured plasma-treated Pd-induced SnO<sub>2</sub>, and Mingming Zhu et al. [11] synthesized Ho-loaded SnO<sub>2</sub> and showed excellent gas-sensing properties due to the generation of oxygen vacancies. In addition to this, few researchers organized nanocomposites such as PdO/SnO<sub>2</sub>/CuO [12], rGO/SnO<sub>2</sub> [13], SnO<sub>2</sub>/NiO [14], and SnO<sub>2</sub>-In<sub>2</sub>O<sub>3</sub> [15] boosted the gas-sensing behavior due to the formation of heterojunction. However, all the mentioned materials have showed gas-sensing response between 100 and 200 °C.

Sensitivity, selectivity, and stability are the three key parameters for measuring gas-sensing properties. Sensitivity is a key feature of a gas sensor that needs to be improved in a low-temperature range. Several researchers have made attempts to enhance the sensitivity and stability of SnO<sub>2</sub> with the doping of certain noble metals. Therefore, nanostructured SnO<sub>2</sub> has been extensively used because of the sensing material attributable to the very huge surface area, availability of ample surface states, and improved surface reactivity [16]. Nonetheless, there are some flaws in SnO<sub>2</sub>-based gas sensor such as poor selectivity, sensitivity, and it needs high-operating temperature. It is worth to mention that the sample operated at a higher temperature will increase the cost of the gas sensor and operated temperature can affect the nanostructure of the material resulting in a poor gas response. Apart from these while sensing the hot material the harmful gases may catch fire easily [17]. So it is always better to fabricate a room-temperature gas sensor. Several approaches, such as doping and morphology, play a crucial role in improving the gas-sensing properties of SnO<sub>2</sub> nanostructure at 300 K [18–22]. Doping alters the structural and opto-electrical nature of the SnO<sub>2</sub>. Rare-earth metals such as Gd, Tb, Y, Nd, and Er were widely used to improve SnO<sub>2</sub> gas sensitivity and selectivity. Moreover, research related to the review of the gas-sensing characteristics of metal oxides doped by rare-earth metals is not detailed enough. Few reports are available for doped SnO<sub>2</sub> sensors and they suggests that rare-earth dopants can considerably improve the response of the SnO<sub>2</sub>-based sensor [23, 24]. Chikhale et al. reported that the co-precipitation synthesized 3% SnO<sub>2</sub>-La nanopowder, which exhibited an improved acetone gas-sensing performance compared to pure SnO<sub>2</sub> [25]. Sankar et al. prepared Ru:SnO<sub>2</sub> thin films for sensing of NH<sub>3</sub> by spray method, in which 10% of Ru-doped films showed the highest response toward ammonia operated at 250 °C [26]. Han Wu et al. studied NH<sub>3</sub> sensing through tin monoxide nanoshells for different ppm levels in which the highest response was achieved for 200 ppm [27]. Li et al. reported that electrospinning-synthesized 0.6% Pr-SnO<sub>2</sub> hollow nanofibers have the highest response of ethanol sensing at 300 °C, compared to pure sample [28].

To our knowledge, for Er-doped SnO<sub>2</sub> thin films that could be operated at room temperature for sensing NH<sub>3</sub> is not available. High-operating temperatures have always been a major

issue for sensing purposes. To detect low-level concentration, fast response and recovery time at 300 K are also important. We prepared SnO<sub>2</sub>:Er thin films using the nebulizer spray pyrolysis (NSP) route for the application of ammonia sensors for the achievement of these objectives. While NSP is one of the best methods to construct thin films for tin oxide compared to other methods like RF sputtering, SILAR, sol-gel method, and chemical bath deposition. It is considered as one of the most convenient methods because of its ease of operation, vacuum less route, easy to add doping elements, uniform coatings on a large area, no need for thermal annealing to get better crystalline films [26, 29]. Hence this work focuses on generating SnO<sub>2</sub>:Er thin films using the NSP technique and its features for the ammonia gas sensor.

## Result and discussions

### Structural analysis

Figure 1 illustrates the XRD pattern of SnO<sub>2</sub>:Er thin films coated with various Er doping concentrations. The XRD peaks of the prepared samples appeared at (110), (101), (200), (211), (220), (310), and (301). These observed diffraction peaks signify the polycrystalline nature of the prepared samples with the rutile tetragonal structure (JCPDS card No. 41-1445). No additional peaks are found corresponding to erbium and erbium oxide. This suggests that the doped material Er<sup>3+</sup> is incorporated well with Sn<sup>4+</sup> lattices. All the films have preferential orientation along with (110) *hkl* planes. A similar phenomenon was reported by Boben Thomas et al. [30] for Ce-doped SnO<sub>2</sub> thin films. From the XRD, it is observed that the intensity of the preferential orientation peaks is decreased and broadened with Er doping concentration increase, which indicates the shrinkage

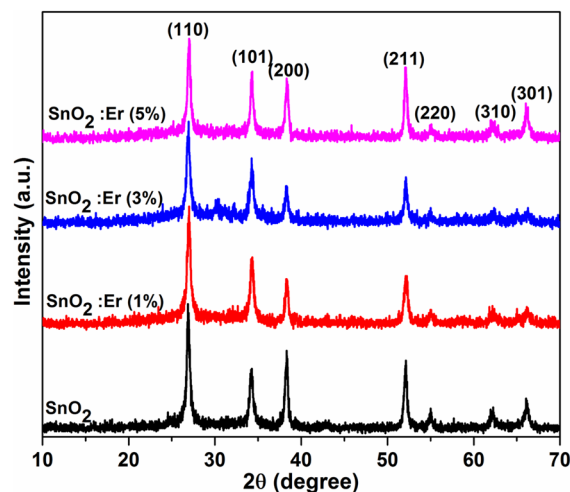


**Figure 1:** X-ray diffraction patterns of SnO<sub>2</sub>:Er thin films with different Er doping concentrations.

of grain size as shown in Fig. S1 (see supporting information). This reduction shows the successful incorporation of the doping element in the host lattice. The grain size of the thin films was evaluated using Debye–Scherer’s equation [31–34],

$$D = \frac{0.9\lambda}{\beta \cos \theta} \quad (1)$$

Here all codes are well-recognized. The determined grain size values are ~ 13, 11, 11, and 10 nm for Er concentration from 0 to 5 wt%, respectively. The lesser grain size gives a bigger surface to volume ration for oxygen adsorption and gas exposure that improves the gas–solid interface possibility, thus improving the response. The lessening in the values of grain size can be attributed to the incorporation of larger ionic radii of Er<sup>3+</sup> ions (0.881 Å) as compared to Sn<sup>4+</sup> ions (0.69 Å) [35]. The reason for peak enlargement can be attributed to the reduction in the size of the grains and the strain present in the lattice due to the expansion of the lattice. This implies that the crystalline nature of the thin films is slightly reduced by adding Er content as well as increase of strain and dislocation density. This indicates that the doping Er content has increased the strain of SnO<sub>2</sub> films in their positions. The decrease in grain size with Er doping is in good agreement with earlier reports of Gurpreet Singh et al. [16] and Conti et al. [36].

The SnO<sub>2</sub> films defects, such as strain ( $\epsilon$ ) and number of dislocations ( $\delta$ ) were estimated using Eqs. (2) and (3) [37–42]:

$$\epsilon = \frac{\beta \cot \theta}{4} \quad (2)$$

$$\delta = \frac{1}{D^2} \quad (3)$$

The calculated structural parameter values of pure SnO<sub>2</sub> and SnO<sub>2</sub>:Er films are given in Table 1. The observed changes of strain due to the point defect and crystallite size are in accordance with literature [43]. The higher  $\epsilon$  and  $\delta$  values noticed on erbium doping indicates the defect generation in films which support for the promotion of vapor sensitivity by NH<sub>3</sub> adsorption due to the defect centers.

Lattice constants “ $a$ ” and “ $c$ ” of the tetragonal phase of SnO<sub>2</sub> and unit cell volume “ $V$ ” were calculated from relations [44, 45]:

$$\frac{1}{d^2} = \left\{ \frac{h^2 + k^2}{a^2} \right\} + \left\{ \frac{l^2}{c^2} \right\} \quad (4)$$

$$V = a^2c \quad (5)$$

where ( $hkl$ ) is miller indices and  $d$  is the inter-planer distance. The lattice constants and unit cell volume values are rising slowly with increasing the Er concentration. The increase of lattice constants “ $a$ ” and “ $c$ ” due to the replacement of Sn<sup>4+</sup> ions by Er<sup>3+</sup> ions introduces stress in the system. The calculated values are listed in Table 1.

### Surface topography analysis

Figure 2 depicts the 3D AFM images of spray pyrolysis-coated SnO<sub>2</sub>:Er films. The pristine and doped SnO<sub>2</sub> thin films have fairly spherical shaped grains along with some bigger grains unevenly spread over the film surface. The roughness of the films was calculated from IA\_9 software installed with the system and noticed to increase as 90, 100, 115, and 120 nm, when Er doping concentrations increase from 0, 1, 3, and 5 wt%, respectively. The film with high roughness promotes the high sensing property.

### Compositional analysis

We have conducted a detailed study on the distribution of elements through EDX and elemental mapping to access the existence of erbium found in SnO<sub>2</sub> thin films. Figure 3a–e displays elemental mapping and EDX image of 5 wt% Er-doped SnO<sub>2</sub> thin film. As can be seen in the result of the elemental mapping in Fig. 3b–d, Sn, Er, and O elements are contained and homogeneously distributed in the erbium-incorporated SnO<sub>2</sub> samples. Since no impurity phases are detected in the XRD spectrum, it suggests that erbium atoms could be integrated into SnO<sub>2</sub> thin films. The weight % of the elements such as Sn = 52.46%, O = 42.73%, and Er = 4.81% is observed from EDX spectrum.

**TABLE 1:** Film thickness, lattice constants, and structural parameters of SnO<sub>2</sub>:Er thin films.

Er concentration (wt%)	Lattice constants (Å)		Cell volume (Å) <sup>3</sup>	Film Thickness (nm)	Crystallite size (nm)	Dislocation density ( $\times 10^{15}$ ) lines m <sup>-2</sup>	Strain ( $\times 10^{-3}$ )
	$a$	$c$					
0	4.6394	3.1561	67.93	580 ± 2	13	5.83	11.36
1	4.6647	3.1591	68.74	550 ± 2	11	7.89	13.26
3	4.6698	3.1648	69.01	540 ± 2	11	8.61	13.89
5	4.6715	3.1687	69.15	520 ± 2	10	10.58	15.41

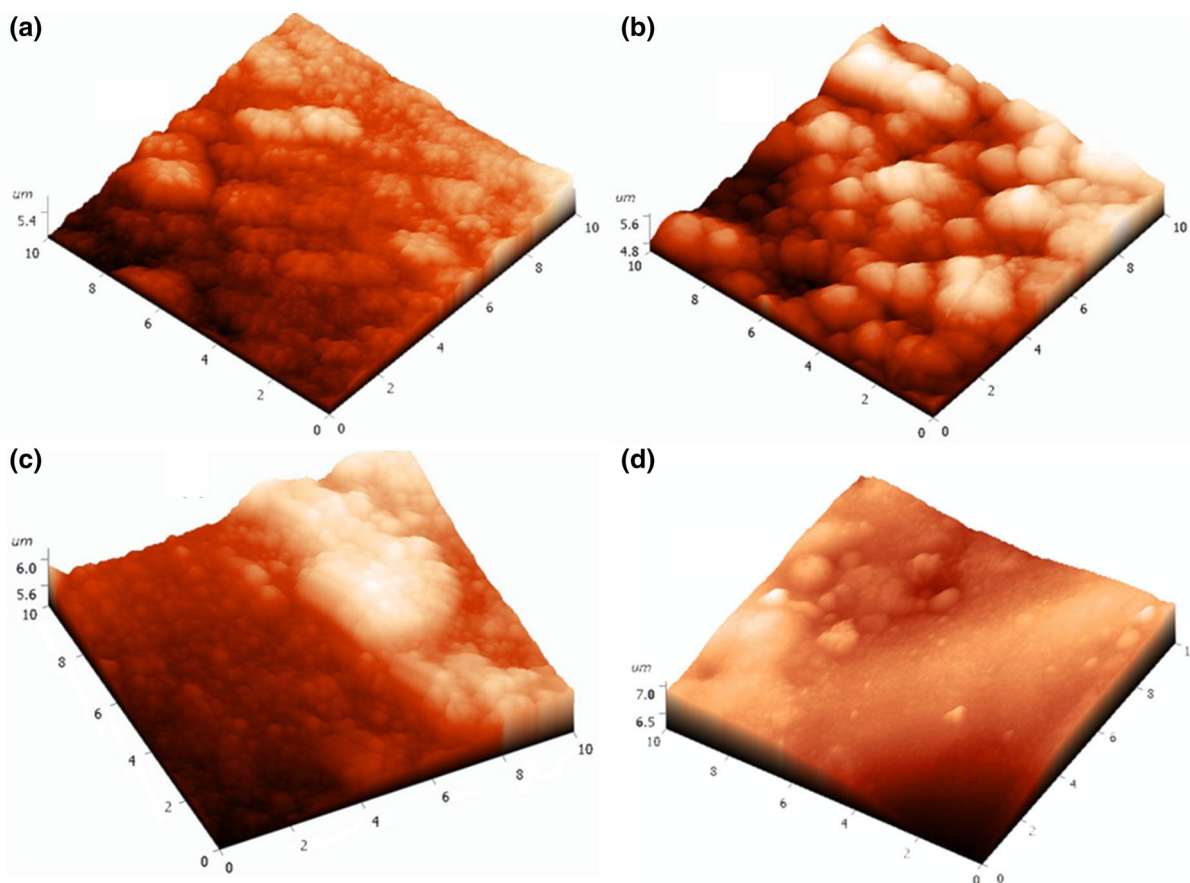


**Figure 2:** AFM 3D images of (a) pure, (b) 1%, (c) 3% and (d) 5% SnO<sub>2</sub>:Er thin films.

### Photoluminescence analysis

Figure 4 displays the room-temperature PL spectra of different doping levels of SnO<sub>2</sub>:Er thin films obtained in the range of 350–600 nm using 325 nm excitation wavelength. The emission spectrum is composed of 365, 402, and 468 nm emission peaks. The peak strength is decreased with the concentration of doping. The near band edge (NBE) emission of SnO<sub>2</sub> is observed at 365 nm (3.39 eV) [46]. The violet peak at 402 nm (3.08 eV) is associated with a doubly ionized oxygen vacancy [47]. The blue peak of 469 nm (2.64 eV) is appeared due to the presence of a singly modified oxygen vacancy [48]. Furthermore, PL intensity is decreased due to a decrease in the crystallinity of the film with increasing doping concentration. These smaller crystallites of the film can promote quick response and recovery time [49].

### UV–Vis analysis

The optical transmittance spectra of SnO<sub>2</sub>:Er thin films is reported in Fig. 5a. The decreasing optical transmittance of the SnO<sub>2</sub>:Er film with increasing Er doping concentration is may be due to an increase in film roughness, which enhances the

gas-sensing property. The optical bandgap ( $E_g$ ) was obtained from Tauc's equation [50, 51]:

$$\alpha hv = A(hv - E_g)^{1/2} \quad (6)$$

where  $\alpha$  is coefficient of absorption,  $\nu$  is frequency of incident photons, and  $E_g$  is energy gap between the valance band and conduction band in the prepared thin films. The optical bandgap ( $E_g$ ) which can be calculated from the extrapolation of the linear section of  $(\alpha hv)^2$  vs.  $hv$  plot. Figure 5b illustrates  $(\alpha hv)^2$  vs. photon energy plots of SnO<sub>2</sub> thin film as a function of Er<sup>3+</sup> doping concentrations. The energy axis intercept gives  $E_g$  values, which is decreased from 3.59 to 3.26 eV with the increase in erbium doping concentrations [52]. This is due to oxygen vacancies like defects created due to smaller grain size [53].

### Ammonia vapor-sensing analysis

In this current investigation, initially, we studied the selectivity of Er-doped SnO<sub>2</sub> thin films through different toxic gases which pollute the environment at room-temperature condition. The NSP prepared samples were subjected to numerous volatile

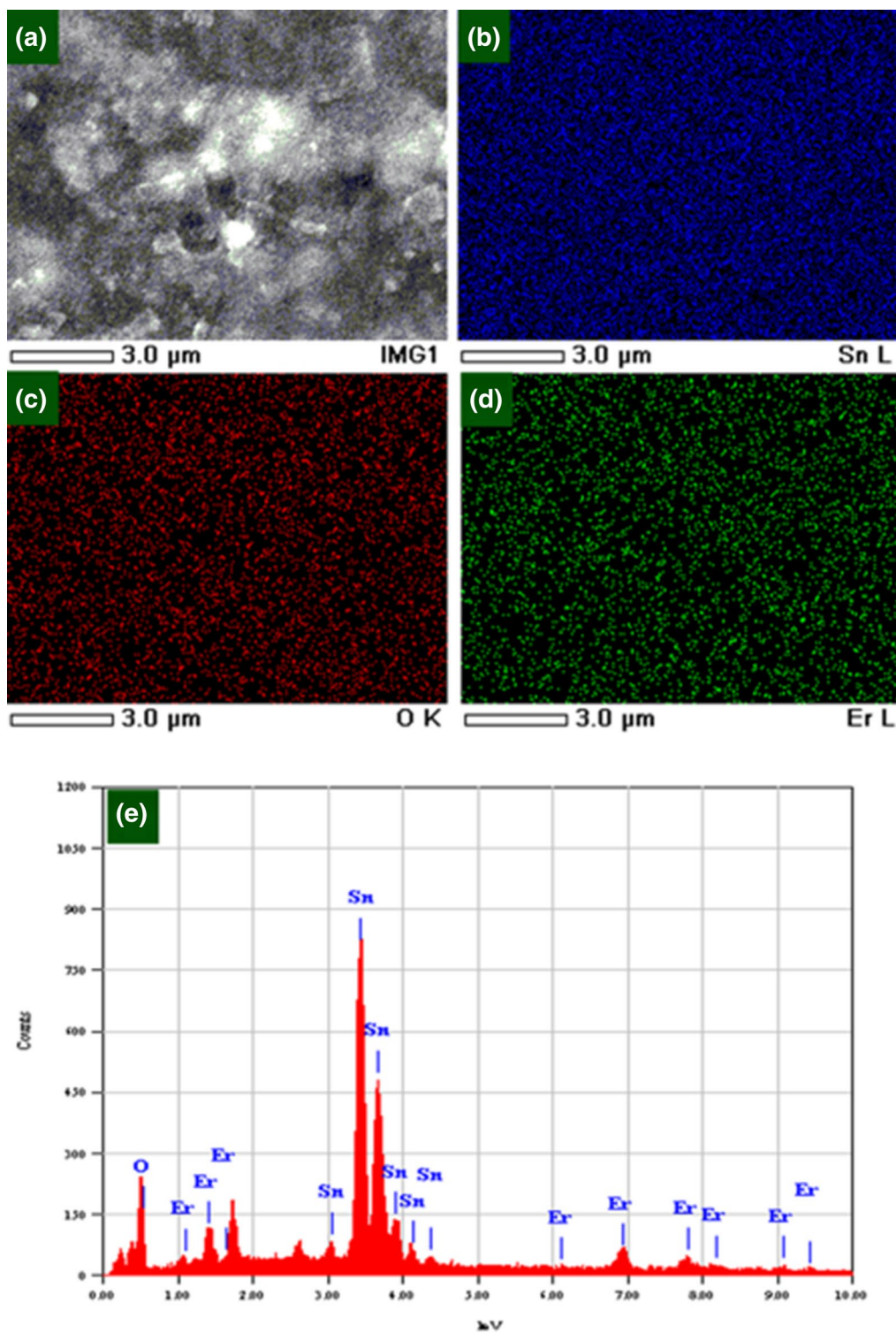
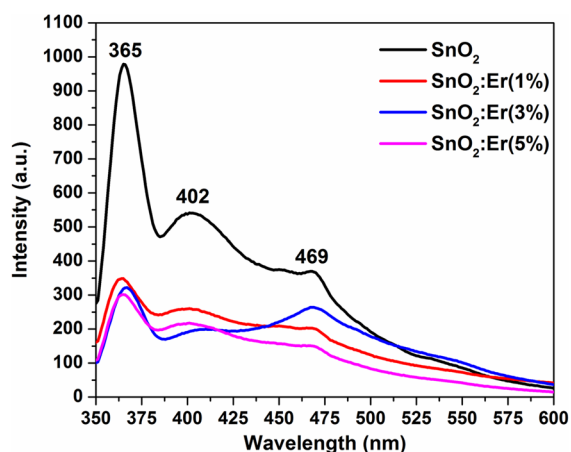


Figure 3: (a) SEM image, (b–d) elemental mapping and (e) EDX spectrum of SnO<sub>2</sub>:Er(5%) thin film.

organic compounds (VOCs) such as toluene (C<sub>7</sub>H<sub>8</sub>), acetone ((CH<sub>3</sub>)<sub>2</sub>CO), isopropanol (C<sub>3</sub>H<sub>8</sub>O), methanol (CH<sub>3</sub>OH), ethanol (C<sub>2</sub>H<sub>5</sub>OH), and ammonia (NH<sub>3</sub>) with the concentration of 25 ppm, are shown in Fig. SII (see supporting information). The

minimum response was observed for toluene (C<sub>7</sub>H<sub>8</sub>), acetone ((CH<sub>3</sub>)<sub>2</sub>CO), isopropanol (C<sub>3</sub>H<sub>8</sub>O), methanol (CH<sub>3</sub>OH), ethanol (C<sub>2</sub>H<sub>5</sub>OH), and the maximum response was observed for ammonia. From this result, we found that the present SnO<sub>2</sub>:Er thin



**Figure 4:** PL spectra of SnO<sub>2</sub>:Er thin films with different Er doping concentrations.

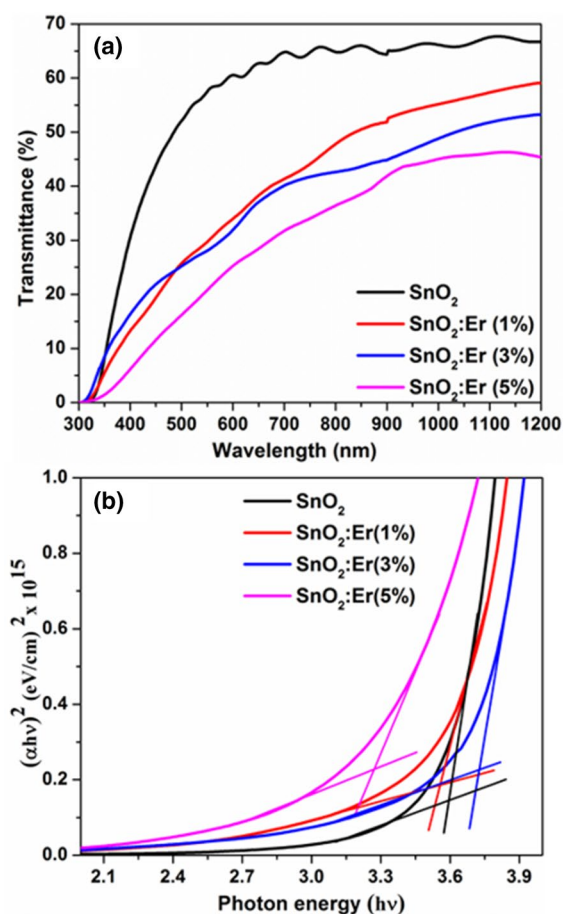


**Figure 5:** (a) Transmission, (b) Tauc's plots of SnO<sub>2</sub>:Er thin films with different Er doping concentrations.

films show a notable response toward ammonia gas. To find out the sensitivity, the prepared Er-doped SnO<sub>2</sub> films were exposed to 25 ppm of NH<sub>3</sub>, at 300 K. The sensitivity versus Er doping concentration for SnO<sub>2</sub>:Er-based sensor is shown in Fig. 6a. A wide

range of sensitivity values of 79, 82, 85, and 91% have been found for SnO<sub>2</sub>-based (Er = 0, 1, 3, and 5%) sensor. This can be due to the formation of nanograins with a rough surface by Er doping, which promotes the inner-grain interaction among gas and film material surface and hence the gas sensitivity has considerably increased. Figure 6b shows the switching behavior of SnO<sub>2</sub> thin film. An analogous switching response of MOs-based sensors for NH<sub>3</sub> was also documented by Khun et al. [54] and Petrov et al. [55]. Figure 6c, d indicates the response ( $t_{res}$ ) and recovery time ( $t_{rec}$ ) properties of SnO<sub>2</sub>:Er films prepared at different doping concentrations (Er = 0, 1, 3, and 5 wt%) toward various NH<sub>3</sub> concentrations. It is evident that  $t_{res}$  and  $t_{rec}$  decrease systematically for Er-doped films and also the  $t_{res}$  decreases, and  $t_{rec}$  rises when increasing the ammonia concentration from 25 to 125 ppm. It can be attributed to an increase in surface roughness and reduction in crystallite size due to Er doping, which greatly promotes the absorption of oxygen on the sensor surface significantly. The obtained response time and recovery time values are shown in comparison Table 2. It indicates 5 wt% Er-doped SnO<sub>2</sub> thin film exhibited rapid response time (~29 s) and quick recovery time (~7 s) toward 25 ppm of ammonia vapor. These obtained values are lower with SnO<sub>2</sub>-based sensor with response/recovery time of 175/210 [54] and 10/30 min [56].

Figure SIII (see supporting information) depicts the sensing features of 5 wt% SnO<sub>2</sub>:Er thin film for various NH<sub>3</sub> contents at room-temperature operating conditions. Sensitivity is increased considerably as ammonia vapor increases from 25 to 125 ppm. The adsorption of higher number of gas fragments and their reaction on surface of SnO<sub>2</sub>:Er(5%) sites may be accountable for high sensitivity to NH<sub>3</sub> gas. The reusability of the sensing sample was analyzed for 5 wt% SnO<sub>2</sub>:Er thin film for 5 cycles and is shown in Fig. SIV (see supporting information). It exhibited good repetition property without an obvious change in their ammonia gas response. The long-term stability of the device is an important parameter for any sensing materials. Figure 7 shows the resistance graph for air and various ppm level of ammonia of pure and SnO<sub>2</sub>:Er films at room temperature observed over 50 days. From this graphical result, we observed that the repeatability and reversibility of the redox reaction on the surface of the film.

### Ammonia gas-sensing mechanism

The sensing nature of gas of SnO<sub>2</sub>:Er films is explainable through oxygen adsorption on surface of SnO<sub>2</sub> by exposure to reducing ammonia vapor. Before NH<sub>3</sub> vapor exposes, the depletion region generated owing to e-trapping by O-molecules and increases the surface resistance of the SnO<sub>2</sub> layer. At the time of NH<sub>3</sub> vapor expose to the surface of the film, which is adsorbed on the SnO<sub>2</sub> surface, a large number of electron-hole pairs produced, thus the carrier concentration in the SnO<sub>2</sub>:Er thin film rises thereby

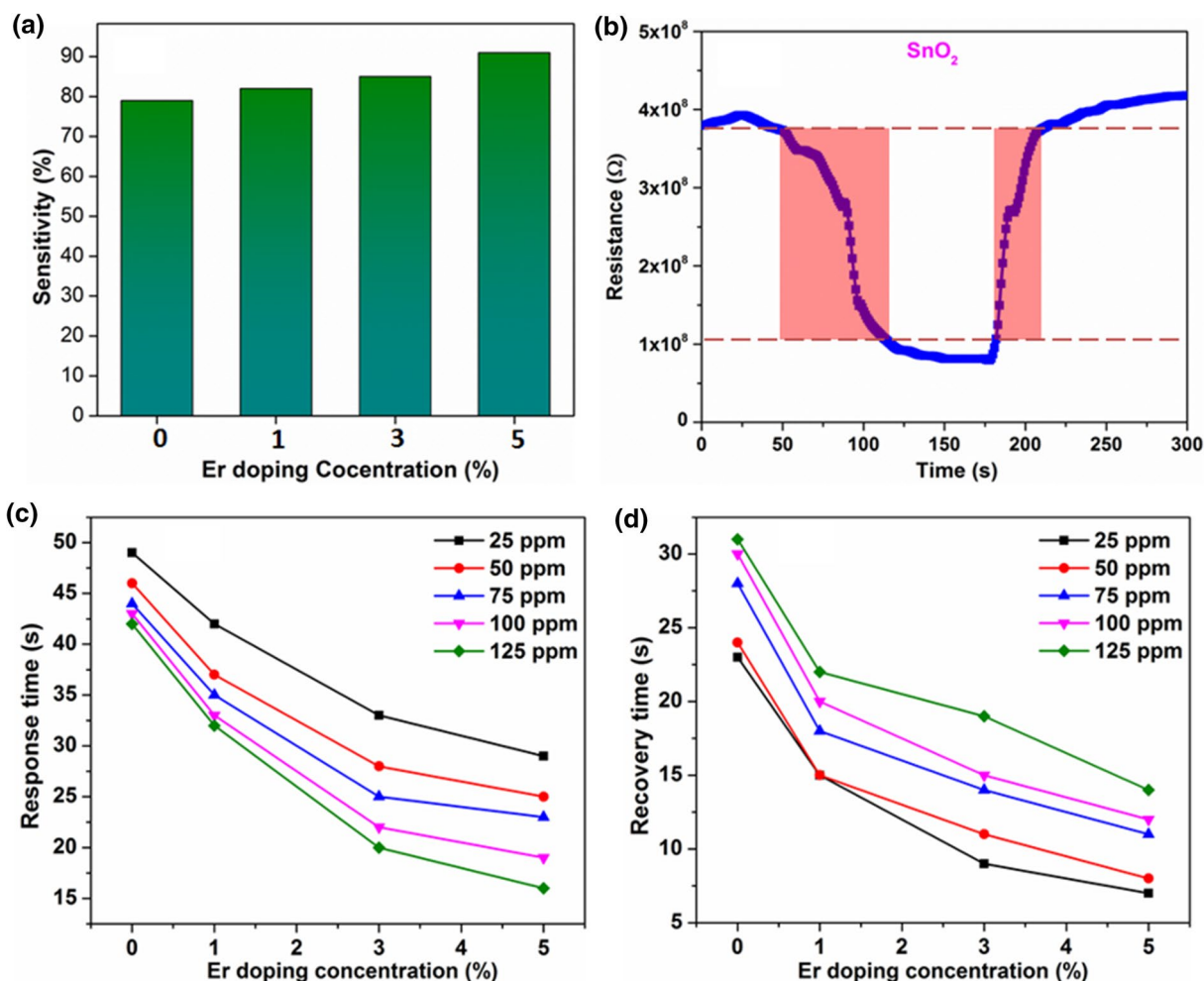
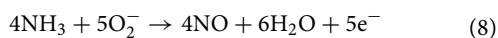
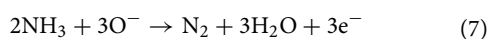


**Figure 6:** (a) Sensitivity, (b) switching behavior of pure SnO<sub>2</sub> film, (c) response time and (d) recovery time toward various concentrations of NH<sub>3</sub> of SnO<sub>2</sub>:Er thin films.

**TABLE 2:** Sensitivity, response, and recovery times of various materials toward NH<sub>3</sub> sensing.

S.No	Material	Concentration/ detection limit	Operating temperature	Response time	Recovery time	Sensitivity (%)	Refs.
1	SnO <sub>2</sub>	50 ppm	250 °C	175 s	210 s	694.4	[54]
2	SnO <sub>2</sub> /Ag	10–250 ppm	20–35 °C			0.01–0.12	[55]
3	SnO <sub>2</sub> /Pt	20–300 ppm	325 °C	10 s	30 s	High	[56]
4	SnO <sub>2</sub> /Fe	1000 ppm	200 °C	–	–	46	[57]
5	Bilayer SnO <sub>2</sub> –WO <sub>3</sub>	250 ppm	300 °C	12 s	58 s	7.1	[58]
7	SnO <sub>2</sub>	3000 ppm	RT	–	–	35	[61]
8	SnO <sub>2</sub> :Er(5%)	25 ppm	RT	29 s	7 s	91	Present work

reducing the depletion region (Fig. 8). The NH<sub>3</sub> oxidation on surface of SnO<sub>2</sub> is given as follows:



Equations (7) and (8) reveal that the free trapped electrons in adsorptive conditions consequences in enhancing of current on reacting the NH<sub>3</sub> with oxygen. Generally, the degree of sensing retort is based on two aspects: (1) quantity of captured

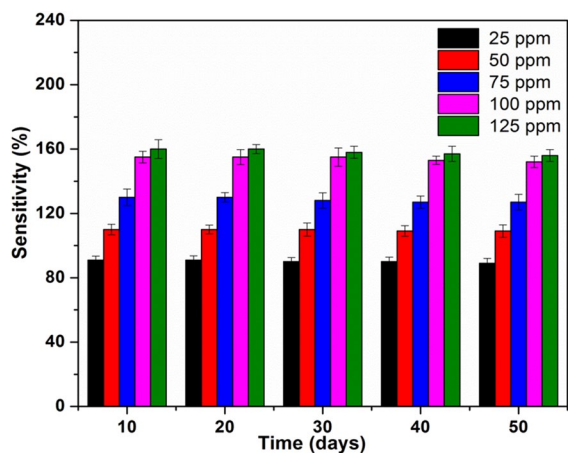


Figure 7: Stability of SnO<sub>2</sub>:Er(5%) thin film tested over a period of 50 days with various concentrations of NH<sub>3</sub>.

electrons from CB by adsorbed oxygen and (2) quantity of released electrons from the oxygen (O) adsorbed on reacting to NH<sub>3</sub>. Based on these facts, nearly all apprehended electrons are freed from adsorbed-O that signify that NH<sub>3</sub> gas can accomplish a central role in exchange of electrons. It is

also interesting to note that at higher levels of Er content the response factor is increased due to the small grain size, rough surface, and high surface area and creation of acceptor level due to replacement of Sn<sup>4+</sup> ions by Er<sup>3+</sup> ions. Petrov et al. [55] proposed a novel mechanism of negative charges transferred from the silver atom to the oxygen because the electronegativity of oxygen is higher than that of silver. Thus a new adsorption active center is created on the surface of the film to promote the sensing property. Rani et al. [57] observed the higher response for high-Fe content in SnO<sub>2</sub> due to the effect of the reduced crystallite size. Tone et al. [58] observed the sensitivity of SnO<sub>2</sub> film is due to the increase of depletion layer thickness by creation of Schottky/p-n junctions and expansion of this layer in the film improving the gas-sensing sensitivity. Shao et al. [59] reported a higher response of the SnO<sub>2</sub> sensor is attributed to the sensitization effects of Sb<sub>2</sub>O<sub>3</sub> and Sb<sub>2</sub>O<sub>5</sub> by Sb doping. In this study, an increased gas sensitivity produced by Er doping is due to low grain size and surface roughness and these factors promote a relatively large number of oxygen ions to be adsorbed and produce high performance.

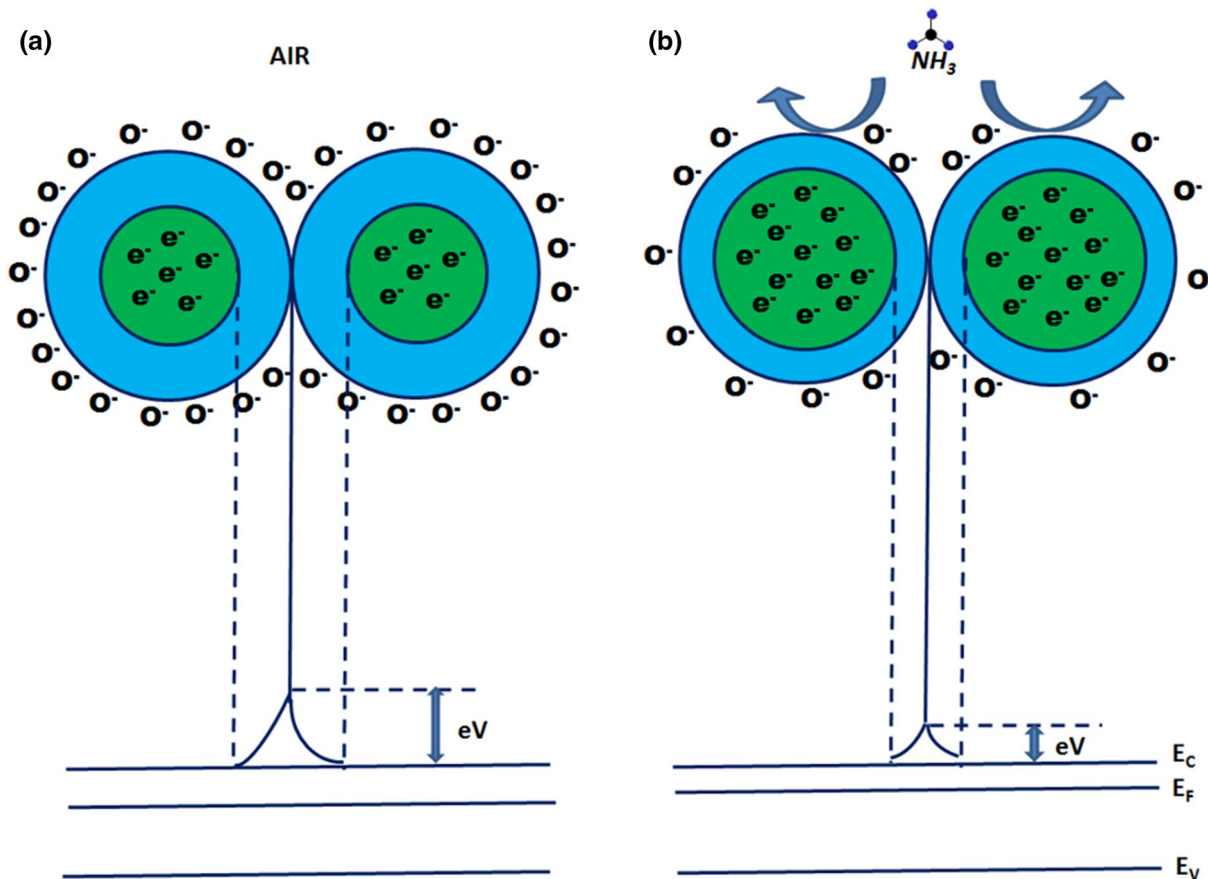


Figure 8: Possible mechanism for the adsorption of (a) air and (b) NH<sub>3</sub> molecules on the SnO<sub>2</sub>:Er surface at room temperature. (Green color spherical shape indicates SnO<sub>2</sub>:Er grain and blue color spherical shape indicates electron depletion layer).



## Conclusion

Rare-earth metal erbium-doped SnO<sub>2</sub> films were fabricated by the NSP method at 400 °C. The XRD, AFM confirms that the Er doping greatly affects the crystallite size and morphology. The ammonia vapor-sensing study was found to be enhanced by Er doping. The SnO<sub>2</sub>:Er (5%) sensor exhibits the highest sensitivity of 91% to 25 ppm of ammonia vapor at room temperature with rapid response and recovery time. These results indicate that SnO<sub>2</sub>:Er (5%) sensor has a potential application for manufacturing a cost-effective and high-performance room-temperature ammonia vapor sensor.

## Experimental section

### Preparation of SnO<sub>2</sub>:Er thin films

Tin(IV) chloride pentahydrate (SnCl<sub>4</sub>·5H<sub>2</sub>O), erbium(III) nitrate pentahydrate (Er N<sub>3</sub>O<sub>9</sub>·5H<sub>2</sub>O), and methanol have been used as a precursor and solvent for preparing the SnO<sub>2</sub>:Er films. The glass substrates were first thoroughly cleaned with distilled water then rinsed with acetone. Finally, the substrates were soaked in chromic acid for 20 min. For the coating of Er-doped SnO<sub>2</sub> thin films, 0.1 M of SnCl<sub>4</sub>·5H<sub>2</sub>O and the required amount of doping material Erbium(III) nitrate pentahydrate (0, 1, 3, and 5 wt%) was added and dissolved in 10 ml of methanol. The precursor solution was continuously stirred for 30 min, and we obtained the homogeneous solution. The formulated solution was sprayed onto a 400 °C pre-heated substrate using a nebulizer spray setup [60]. Once the precursor solution is sprayed on a hot substrate, the thin film was formed by pyrolytic decompose and chemical reactions.

### Characterization techniques

The following characteristic studies were carried to study structure, morphology, and other characteristics of SnO<sub>2</sub>:Er films. Table SI (see supporting information) displays the list of instruments and their parameters applied in current study. The output of the SnO<sub>2</sub>:Er thin-film ammonia vapor sensor was measured in the room-temperature test chamber. The registered quantity of ammonia vapor was sent into test chamber and resistance was measured by the Keithley electrometer w.r.t. time at various concentrations of Er doping. The sensor sensitivity was determined by following equation [54]:

$$\text{Sensitivity} = \left\{ \frac{R_a - R_g}{R_a} \right\} \times 100\% \quad (9)$$

where  $R_a$  and  $R_g$  reflect resistance in air and gas atmospheric testing, respectively. In this case, the time of response of the prepared sensor is determined by means of time needed for

resistance to exceed 90% of the steadiness value once the ammonia gas is applied and time of recovery is recorded by means of time essential for sensor to achieve 10% resistance higher than unique value in air.

## Acknowledgments

The authors extend their sincere appreciation to the Dean-ship of Scientific Research at Princess Nourah bint Abdulrahman University for funding this research through the Fast-track Research Funding Program.

## Compliance with ethical standards

**Conflict of interest** Authors declare no conflict of interest in current work.

## Supplementary information

The online version contains supplementary material available at <https://doi.org/10.1557/s43578-020-00033-0>.

## References

1. S. Farzi-kahkesh, M.B. Rahmani, A. Fattah, Growth of novel  $\alpha$ -MoO<sub>3</sub> hierarchical nanostructured thin films for ethanol sensing. *Mater. Sci. Semicond. Process.* **120**, 105263 (2020)
2. Y. Cui, M. Zhang, X. Li, B. Wang, R. Wang, Investigation on synthesis and excellent gas-sensing properties of hierarchical Au-loaded SnO<sub>2</sub> nanoflowers. *J. Mater. Res.* **34**, 2944 (2019)
3. R.P. Patil, S.S. Gaikwad, A.N. Karanjekar, P.K. Khanna, G.H. Jain, V.B. Gaikwad, P.V. More, N. Bisht, Optimization of strontium-doping concentration in BaTiO<sub>3</sub> nanostructures for room temperature NH<sub>3</sub> and NO<sub>2</sub> gas sensing. *Mater. Today Chem.* **16**, 100240 (2020)
4. J. Hu, X. Li, X. Wang, Y. Li, Q. Li, F. Wang, Hierarchical aloe-like SnO<sub>2</sub> nanoflowers and their gas sensing properties. *J. Mater. Res.* **33**, 1433 (2018)
5. C. Bouzidi, H. Elhouichet, A. Moadhen, Yb<sup>3+</sup> effect on the spectroscopic properties of Er–Yb codoped SnO<sub>2</sub> thin films. *J. Lumin.* **131**, 2630 (2011)
6. T.T. Van, N. Truc Ly, L.T. Giang, C.T. My Dung, Tin dioxide nanocrystals as an effective sensitizer for erbium ions in Er-doped SnO<sub>2</sub> systems for photonic applications. *J. Nanomater.* **2016**, 1 (2016)
7. B. Yulianto, G. Gumilar, N.L.W. Septiani, SnO<sub>2</sub> nanostructure as pollutant gas sensors: synthesis, sensing performances, and mechanism. *Adv. Mater. Sci. Eng.* (2015). <https://doi.org/10.1155/2015/694823>
8. J. Ma, Y. Liu, H. Zhang, P. Ai, N. Gong, Y. Zhang, Synthesis and high sensing properties of a single Pd-doped SnO<sub>2</sub> nanoribbon. *Nanoscale Res. Lett.* **9**, 503 (2014)

9. J.-H. Kim, A. Mirzaei, J.-Y. Kim, J.-H. Lee, H.W. Kim, S. Hishita, S.S. Kim, Enhancement of gas sensing by implantation of Sb-ions in SnO<sub>2</sub> nanowires. *Sens. Actuators B* **304**, 127307 (2020)
10. K. Hu, F. Wang, H. Liu, Y. Li, W. Zeng, Enhanced hydrogen gas sensing properties of Pd-doped SnO<sub>2</sub> nanofibres by Ar plasma treatment. *Ceram. Int.* **46**, 1609 (2020)
11. M. Zhu, T. Yang, C. Zhai, L. Du, J. Zhang, M. Zhang, Fast triethylamine gas sensing response properties of Ho-doped SnO<sub>2</sub> nanoparticles. *J. Alloys Compd.* **817**, 152724 (2020)
12. S. Javanmardi, S. Nasresfahani, M.H. Sheikhi, Facile synthesis of PdO/SnO<sub>2</sub>/CuO nanocomposite with enhanced carbon monoxide gas sensing performance at low operating temperature. *Mater. Res. Bull.* **118**, 110496 (2019)
13. A. Choudhari, B.A. Bhanvase, V.K. Saharan, P.H. Salame, Y. Hunge, Sonochemical preparation and characterization of rGO/SnO<sub>2</sub> nanocomposite: electrochemical and gas sensing performance. *Ceram. Int.* **46**(8, Part A), 11290 (2020)
14. L. Xu, M. Ge, F. Zhang, H. Huang, Y. Sun, D. He, Nanostructured of SnO<sub>2</sub>/NiO composite as a highly selective formaldehyde gas sensor. *J. Mater. Res.* (2020). <https://doi.org/10.1557/jmr.2020.239>
15. G.N. Gerasimov, V.F. Gromov, M.I. Ikim, O.J. Ilegbusi, S.A. Ozerin, L.I. Trakhtenberg, Structure and gas-sensing properties of SnO<sub>2</sub>-In<sub>2</sub>O<sub>3</sub> nanocomposites synthesized by impregnation method. *Sens. Actuators B* **320**, 128406 (2020)
16. G. Singh, Virpal, R.C. Singh, Highly sensitive gas sensor based on Er-doped SnO<sub>2</sub> nanostructures and its temperature dependent selectivity towards hydrogen and ethanol. *Sens. Actuators B* **282**, 373 (2019)
17. Z.S. Hosseini, A.I. Zad, A. Mortezaali, Room temperature H<sub>2</sub>S gas sensor based on rather aligned ZnO nanorods with flower-like structures. *Sens. Actuators B* **207**, 865 (2015)
18. Z. Lin, N. Li, Z. Chen, P. Fu, The effect of Ni doping concentration on the gas sensing properties of Ni doped SnO<sub>2</sub>. *Sens. Actuators B* **239**, 501 (2017)
19. N.M. Shaalan, T. Yamazaki, T. Kikuta, Influence of morphology and structure geometry on NO<sub>2</sub> gas-sensing characteristics of SnO<sub>2</sub> nanostructures synthesized via a thermal evaporation method. *Sens. Actuators B* **153**, 11 (2011)
20. Y. Chen, L. Yu, D. Feng, M. Zhuo, M. Zhang, E. Zhang, Z. Xu, Q. Li, T. Wang, Superior ethanol-sensing properties based on Ni-doped SnO<sub>2</sub> p-n heterojunction hollow spheres. *Sens. Actuators B* **166-167**, 61 (2012)
21. Y. Lin, W. Wei, Y. Li, F. Li, J. Zhou, D. Sun, Y. Chen, S. Ruan, Preparation of Pd nanoparticle-decorated hollow SnO<sub>2</sub> nanofibers and their enhanced formaldehyde sensing properties. *J. Alloys Compd.* **651**, 690 (2015)
22. L. Xiao, S. Shu, S. Liu, A facile synthesis of Pd-doped SnO<sub>2</sub> hollow microcubes with enhanced sensing performance. *Sens. Actuators B* **221**, 120 (2015)
23. Y. Zhao, Y. Li, W. Wan, X. Ren, H. Zhao, Surface defect and gas-sensing performance of the well-aligned Sm-doped SnO<sub>2</sub> nanoarrays. *Mater. Lett.* **218**, 22 (2018)
24. G. Qin, F. Gao, Q. Jiang, Y. Li, Y. Liu, L. Luo, K. Zhao, H. Zhao, Well-aligned Nd-doped SnO<sub>2</sub> nanorod layered arrays: preparation, characterization and enhanced alcohol-gas sensing performance. *Phys. Chem. Chem. Phys.* **18**, 5537 (2016)
25. L. Chikhale, J. Patil, A. Rajgure, F. Shaikh, I. Mulla, S. Suryavanshi, Structural, morphological and gas sensing properties of undoped and Lanthanum doped nanocrystalline SnO<sub>2</sub>. *Ceram. Int.* **40**, 2179 (2014)
26. C. Sankar, V. Ponnuswamy, M. Manickam, R. Mariappan, R. Suresh, Structural, morphological, optical and gas sensing properties of pure and Ru doped SnO<sub>2</sub> thin films by nebulizer spray pyrolysis technique. *Appl. Surf. Sci.* **349**, 931 (2015)
27. H. Wu, Z. Ma, Z. Lin, H. Song, S. Yan, Y. Shi, High-sensitive ammonia sensors based on tin monoxide nanoshells. *Nanomaterials* **9**(3), 388 (2019)
28. W.Q. Li, S.Y. Ma, Y.F. Li, X.B. Li, C.Y. Wang, X.H. Yang, L. Cheng, Y.Z. Mao, J. Luo, D.J. Gengzang, G.X. Wan, X.L. Xu, Preparation of Pr-doped SnO<sub>2</sub> hollow nanofibers by electrospinning method and their gas sensing properties. *J. Alloys Compd.* **605**, 80 (2014)
29. S. Palanichamy, J. Raj Mohamed, K. Deva Arun Kumar, P.S. Satheesh Kumar, S. Pandiaraj, L. Amalraj, Physical properties of rare earth metal (Gd<sup>3+</sup>) doped SnO<sub>2</sub> thin films prepared by simplified spray pyrolysis technique using nebulizer. *Optik* **194**, 162887 (2019)
30. B. Thomas, S. Deepa, K. Prasanna Kumari, Influence of surface defects and preferential orientation in nanostructured Ce-doped SnO<sub>2</sub> thin films by nebulizer spray deposition for lowering the LPG sensing temperature to 150 °C. *Ionics* **25**, 809 (2019)
31. H.H. Ahmed, Variation of the structural, optical and electrical properties of CBD CdO with processing temperature. *Mater. Sci. Semicond. Process.* **66**, 215 (2017)
32. M. Shkir, S. AlFaify, Tailoring the structural, morphological, optical and dielectric properties of lead iodide through Nd<sup>3+</sup> doping. *Sci. Rep.* **7**, 16091 (2017)
33. M. Shkir, S. Kushwaha, K. Maurya, G. Bhagavannarayana, M. Wahab, Characterization of ZnSe nanoparticles synthesized by microwave heating process. *Solid State Commun.* **149**, 2047 (2009)
34. M. Shkir, S. AlFaify, Effect of Gd<sup>3+</sup> doping on structural, morphological, optical, dielectric, and nonlinear optical properties of high-quality PbI<sub>2</sub> thin films for optoelectronic applications. *J. Mater. Res.* **34**(16), 2765 (2019)
35. K.R. Devi, G. Selvan, M. Karunakaran, K. Kasirajan, NH<sub>3</sub> sensor based SILAR coated undoped and aluminium doped ZnO thin films. *Comp. Eng. J.* **11**, 249 (2020)

36. T.G. Conti, A.J. Chiquito, E.R. Leite, Electrical properties of SnO<sub>2</sub>: Sb ultrathin films prepared by colloidal deposition process. *J. Mater. Res.* **31**, 148 (2016)
37. C.S. Prajapati, P.P. Sahay, Effect of precursors on structure, optical and electrical properties of chemically deposited nanocrystalline ZnO thin films. *Appl. Surf. Sci.* **258**, 2823 (2012)
38. M. Ali Yıldırım, A. Ateş, Influence of films thickness and structure on the photo-response of ZnO films. *Opt. Commun.* **283**, 1370 (2010)
39. M. Shkir, M. Anis, S.S. Shaikh, M.S. Hamdy, S. AlFaify, Impact of Se doping on optical and third-order nonlinear optical properties of spray pyrolysis fabricated CdS thin films for optoelectronics. *Appl. Phys. B* **126**, 121 (2020)
40. M. Shkir, I.S. Yahia, M. Kilany, M.M. Abutalib, S. AlFaify, R. Darwish, Facile nanorods synthesis of KI:HAp and their structure-morphology, vibrational and bioactivity analyses for biomedical applications. *Ceram. Int.* **45**, 50 (2019)
41. M. Shkir, M. Kilany, I.S. Yahia, Facile microwave-assisted synthesis of tungsten-doped hydroxyapatite nanorods: a systematic structural, morphological, dielectric, radiation and microbial activity studies. *Ceram. Int.* **43**, 14923 (2017)
42. M. Shkir, K.V. Chandekar, T. Alshahrani, A. Kumar, S. AlFaify, A novel terbium doping effect on physical properties of lead sulfide nanostructures: a facile synthesis and characterization. *J. Mater. Res.* (2020). <https://doi.org/10.1557/jmr.2020.216>
43. V. Mote, Y. Purushotham, B. Dole, Williamson–Hall analysis in estimation of lattice strain in nanometer-sized ZnO particles. *J. Theoret. Appl. Phys.* **6**, 6 (2012)
44. R. Mariappan, V. Ponnuswamy, P. Suresh, R. Suresh, M. Ragavendar, C. Sankar, Deposition and characterization of pure and Cd doped SnO<sub>2</sub> thin films by the nebulizer spray pyrolysis (NSP) technique. *Mater. Sci. Semicond. Process.* **16**, 825 (2013)
45. S. Maheswari, M. Karunakaran, K. Kasirajan, Nebuliser spray pyrolysis coated undoped and Tb-doped SnO<sub>2</sub> thin films: ammonia vapour sensor application. *Sustain. Humanosphere* **16**, 1136 (2020)
46. S.K. Sinha, R. Bhattacharya, S.K. Ray, I. Manna, Influence of deposition temperature on structure and morphology of nanostructured SnO<sub>2</sub> films synthesized by pulsed laser deposition. *Mater. Lett.* **65**, 146 (2011)
47. S. Chen, X. Zhao, H. Xie, J. Liu, L. Duan, X. Ba, J. Zhao, Photoluminescence of undoped and Ce-doped SnO<sub>2</sub> thin films deposited by sol–gel-dip-coating method. *Appl. Surf. Sci.* **258**, 3255 (2012)
48. K. Ravichandran, K. Thirumurugan, Type inversion and certain physical properties of spray pyrolysed SnO<sub>2</sub>: Al films for novel transparent electronics applications. *J. Mater. Sci. Technol.* **30**, 97 (2014)
49. A.N.G. Krishnan, G.K. Mani, P. Shankar, B. Vutukuri, J.B.B. Rayappan, Gas sensing characteristics of nanostructured ZnO thin film-influence of manganese doping. *Chem. Sens.* **5**, 9 (2015)
50. M. Thirumoorthi, J.T.J. Prakash, A study of Tin doping effects on physical properties of CdO thin films prepared by sol–gel spin coating method. *J. Asian Ceram. Soc.* **4**, 39 (2016)
51. M. Shkir, K.V. Chandekar, A. Khan, A.M. El-Toni, S. AlFaify, A facile synthesis of Bi@PbS nanosheets and their key physical properties analysis for optoelectronic technology. *Mater. Sci. Semicond. Process.* **107**, 104807 (2020)
52. S. Munir, S.M. Shah, H. Hussain, R. Ali khan, Effect of carrier concentration on the optical band gap of TiO<sub>2</sub> nanoparticles. *Mater. Des.* **92**, 64 (2016)
53. V.B. Kamble, A.M. Umarji, Defect induced optical bandgap narrowing in undoped SnO<sub>2</sub> nanocrystals. *AIP Adv.* **3**, 082120 (2013)
54. K.K. Khun, A. Mahajan, R.K. Bedi, SnO<sub>2</sub> thick films for room temperature gas sensing applications. *J. Appl. Phys.* **106**, 124509 (2009)
55. V.V. Petrov, T.N. Nazarova, A.N. Korolev, N.F. Kopilova, Thin sol–gel SiO<sub>2</sub>–SnO<sub>x</sub>–AgO<sub>y</sub> films for low temperature ammonia gas sensor. *Sens. Actuators B* **133**, 291 (2008)
56. O. Anisimov, N. Maksimova, E. Chernikov, E. Sevastyanov, N. Sergeychenko: Sensitivity to NH<sub>3</sub> of SnO<sub>2</sub> thin films prepared by magnetron sputtering, in *2009 International Siberian Conference on Control and Communications*, (IEEE, City, 2009), pp. 189
57. S. Rani, S.C. Roy, M.C. Bhatnagar, Effect of Fe doping on the gas sensing properties of nano-crystalline SnO<sub>2</sub> thin films. *Sens. Actuators B* **122**, 204 (2007)
58. N.V. Toan, C.M. Hung, N.V. Duy, N.D. Hoa, D.T.T. Le, N.V. Hieu, Bilayer SnO<sub>2</sub>–WO<sub>3</sub> nanofilms for enhanced NH<sub>3</sub> gas sensing performance. *Mater. Sci. Eng. B* **224**, 163 (2017)
59. S. Shao, R. Koehn, H. Wu, T. Wu, W.-F. Rao, Generation of highly ordered nanoporous Sb–SnO<sub>2</sub> thin films with enhanced ethanol sensing performance at low temperature. *Sens. Actuators B* **145**, 847 (2010)
60. R. Mariappan, V. Ponnuswamy, P. Suresh, Effect of doping concentration on the structural and optical properties of pure and tin doped zinc oxide thin films by nebulizer spray pyrolysis (NSP) technique. *Superlattices Microstruct.* **52**, 500 (2012)
61. M.H. Diwan, W.M. Kadem, Z.T. Khodair, Effect of modified SnO<sub>2</sub> film surface on the ammonia gas sensitivity at room temperature, in *AIP Conference Proceedings*, (2144, AIP Publishing LLC, City, 2019), p. 030010